Redox Biology 38 (2021) 101792

Contents lists available at ScienceDirect

Redox Biology

journal homepage: www.elsevier.com/locate/redox

FUNDC1-dependent mitophagy induced by tPA protects neurons against cerebral ischemia-reperfusion injury

Ying Cai [a], Eryan Yang [a,b,c], Xiuhua Yao [a], Xuebin Zhang [d], Qixue Wang [e], Yunfei Wang [e], Ji Liu [b], Weijia Fan [a], Kaikai Yi [c,e], Chunsheng Kang [e,**], Jialing Wu [a,b,*]

[a] Tianjin Key Laboratory of Cerebral Vascular and Neurodegenerative Diseases, Tianjin Neurosurgical Institute, Tianjin Huanhu Hospital, Tianjin, 300350, China
[b] Department of Neurology, Tianjin Huanhu Hospital, Tianjin, 300350, China
[c] Graduate School of Tianjin Medical University, Tianjin, 300070, China
[d] Department of Pathology, Tianjin Huanhu Hospital, Tianjin, 300350, China
[e] Department of Neurosurgery, Tianjin Medical University General Hospital, Lab of Neuro-oncology, Tianjin Neurological Institute, Key Laboratory of Post-Neuroinjury Neuro-repair and Regeneration in Central Nervous System, Tianjin, 300052, China

ARTICLE INFO

Keywords:
tPA
Ischemia-reperfusion
CRISPR/Cas9
FUNDC1
Mitophagy

ABSTRACT

Autophagy of mitochondria, termed mitophagy, plays an important role in cerebral ischemia-reperfusion (IR) injury, but the mechanism is not yet clear. Tissue-type plasminogen activator (tPA) is the most important thrombolytic drug in the clinical treatment of ischemic stroke and has neuroprotective effects. Here, we explored the effects of tPA on neuronal apoptosis and mitophagy following IR. We found that knocking out the tPA gene significantly aggravated brain injury and increased neuronal apoptosis and mitochondrial damage. Exposure of neurons to tPA reduced injury severity and protected mitochondria. Further studies demonstrated that this protective effect of tPA was achieved via regulation of FUNDC1-mediated mitophagy. Furthermore, we found that tPA enhanced the expression level of FUNDC1 by activating the phosphorylation of AMPK. In summary, our results confirm that tPA exerts neuroprotective effects by increasing the phosphorylation of AMPK and the expression of FUNDC1, thereby inhibiting apoptosis and improving mitochondrial function.

1. Introduction

As the only clinical thrombolytic drug approved by the FDA, tissue-type plasminogen activator (tPA) plays an important role in the treatment of ischemic stroke during the super-early stage. In addition to its thrombolytic effect in blood vessels, recent evidence indicates that tPA has neuroprotective effects [1,2]. tPA is widely expressed in the hippocampus, cerebellum and other brain regions and controls many cerebral physiological processes, such as neuronal migration, glutamatergic neurotransmission, neurite outgrowth, synaptic plasticity, long-term potentiation, neurovascular coupling and anxiety [2–5]. An increasing number of studies have shown that tPA is a neuroprotector in the response to acute ischemic injury in the brain [6].

Mitochondrial injury associated with blood flow recovery is an important pathophysiological process after ischemia-reperfusion (IR). Functionally damaged mitochondria and reactive oxygen species (ROS)

Schematic representation of key mechanisms underpinning tPA-mediated protection of neurons against IR via FUNDC1-dependent mitophagy. As pictured in the left-hand path, IR injury is associated with decreases in endogenous tPA that lead to mitochondrial damage. Cytochrome C is then released into the cytoplasm, triggering a caspase cascade reaction and neuronal apoptosis. At the same time, the mitochondrial damage results in FUNDC1 degradation, preventing FUNDC1 from binding to free LC3 effectively and resulting in inhibition of mitochondrial autophagy. As pictured in the right-hand path, addition of exogenous tPA following IR leads to increased AMPK phosphorylation and FUNDC1 expression. FUNDC1 binds to LC3 through its LIR domain, causing an autophagic bilayer membrane to envelop mitochondria, inducing mitophagy. The resulting mitophagy inhibits apoptosis and protects neurons.

* Corresponding author. Tianjin Key Laboratory of Cerebral Vascular and Neurodegenerative Diseases, Tianjin Neurosurgical Institute, Department of Neurology, Tianjin Huanhu Hospital, 6 Jizhao Road, Jinnan District, Tianjin, 300350, China.
** Corresponding author. Department of Neurosurgery, Tianjin Medical University General Hospital; Lab of Neuro-oncology, Tianjin Neurological Institute, Key Laboratory of Post-Neuroinjury Neuro-repair and Regeneration in Central Nervous System, 154 Anshan Road, Heping District, Tianjin, 300052, China.
E-mail addresses: kang97061@tmu.edu.cn (C. Kang), wywjl2009@nankai.edu.cn (J. Wu).

https://doi.org/10.1016/j.redox.2020.101792
Received 1 May 2020; Received in revised form 13 October 2020; Accepted 3 November 2020
Available online 7 November 2020

Abbreviations

IR	ischemia-reperfusion
tPA	tissue-type plasminogen activator
FUNDC1	FUN14 domain-containing 1
AMPK	AMP-activated protein kinase
ROS	reactive oxygen species
LIR	LC3-interacting region
CNS	central nervous system
OGD	oxygen-glucose deprivation
CRISPR	clustered regularly interspaced short palindromic repeats
sgRNA	small guide RNA
MOI	multiplicity of infection
MTT	3-(4,5-dimethyl-2-thiazolyl)-2,5-diphenyl-2H-tetrazolium bromide
PMSF	phenylmethylsulfonyl fluoride
BCA	bicinchoninic acid
CytC	cytochrome C
PI	propidium iodide
MCAO	middle cerebral artery occlusion
mNSS	Modified Neurological Severity Score
TTC	2,3,5-triphenyl-tetrazolium chloride
TUNEL	terminal deoxynucleotidyl transferase-mediated dUTP-biotin nick end labeling
PPI	protein-protein interaction
KEGG	Kyoto Encyclopedia of Genes and Genomes
OE	overexpression
DM	dorsomorphin

produced by mitochondrial oxidative stress can be used as substrates to induce autophagy [7], which can recycle or degrade proteins and damaged organelles in various diseases [8]. Mitophagy is a selective autophagy process that specifically degrades damaged mitochondria to enable their components to be reused. Through selective removal and degradation of damaged or superfluous mitochondria, mitophagy prevents the accumulation of mitochondrial DNA mutations and reprograms cellular metabolism [9]. Mitophagy plays an important role in cerebral IR injury, but the mechanism is not yet clear. FUN14 domain-containing 1 (FUNDC1), a three-transmembrane protein localized on the outer mitochondrial membrane, is a mammalian mitophagy receptor. FUNDC1 has an LC3-interacting region (LIR) and mainly mediates ischemia-induced mitophagy by interacting with and recruiting LC3 to mitochondria [10].

ATP is the predominant energy source for brain biological activity and is depleted under ischemic conditions. AMP-activated protein kinase (AMPK) is distinctly expressed in the central nervous system (CNS), which makes the brain susceptible to ischemic stroke. AMPK is activated in response to stress factors and regulates the supply of ATP [11]. AMPK plays a crucial role in IR to preserve energy homeostasis by regulating apoptosis, glutamate excitotoxicity, mitochondrial dysfunction and autophagy; these functions suggest AMPK as a potential therapeutic target for ischemic stroke [12].

Recently, tPA has been reported to perceive oxidative stress during IR, enhance phosphorylation of AMPK, increase glucose uptake in neurons, and promote mitochondrial ATP production [13,14]. However, how tPA perceives oxidative stress during IR and reduces mitochondrial damage has not been reported. Therefore, we sought to explore whether tPA protects neurons by maintaining mitochondrial function and to investigate whether FUNDC1-mediated mitophagy plays a role in this process.

2. Materials and methods

2.1. Cell culture and IR injury model

The mouse hippocampal neuron cell line HT22 (Ginio, Guangzhou, China) and brain microvascular endothelial cell line bEnd.3 were cultured in Dulbecco's modified Eagle's medium (DMEM) containing 10% fetal bovine serum and 1% penicillin-streptomycin (Thermo Fisher, MA, USA). The cells in the control group were not treated. Cells subjected to IR injury were first cultured in DMEM without glucose in an anaerobic incubator at 37 °C under 5% CO_2 and <1% O_2 (oxygen-glucose deprivation, OGD). After ischemic injury, glucose and sodium pyruvate were added to the culture medium, and the cells were cultured at 37 °C under 5% CO_2 for reperfusion. A subgroup of IR cells was incubated with a final concentration of 5 nM tPA (Molecular Innovations, MI, USA) at the beginning of IR.

2.2. CRISPR/Cas9 system and sequencing

The CRISPR/Cas9 gene-editing system (GeneChem, Shanghai, China) was used to generate $tPA^{-/-}$ cells. The sgRNA sequence TGCACCGGCAATATTCCACC was cloned into the LV-sgNeomycin vector to produce the lentivirus-sgRNA construct. In addition, the Lenti-CAS9-Puro vector was used to produce the lentivirus-Cas9 construct.

First, cultured HT22 cells were infected with lentivirus-Cas9 at a multiplicity of infection (MOI) of 5 and screened with puromycin for 1–2 weeks to obtain stable Cas9-HT22 cells. Then, Cas9-HT22 cells were infected with lentivirus-sgRNA and screened with neomycin. After 1–2 weeks, the monoclonal cells were screened. After 100 μL of medium was added to all wells in a 96-well plate except the first well (A1), the cells were collected and adjusted to 1000 cells/mL, and 200 μL of cells were seeded into the first well of the 96-well plate. Then, 100 μL was transferred from well A1 to well B1 and mixed gently. Such 1:2 dilutions were performed down the entire column, and 100 μL was discarded from well H1. An additional 100 μL of medium was added to each well in column 1, and then 1:2 dilutions were repeated in order down each row; 100 μL was discarded from each of the wells in the last column (A12 through H12) so that each well ultimately contained 100 μL of cell suspension. All the wells were observed under a microscope, and the wells with only one cell were labeled. The plate was cultured in a cell incubator until monoclonal cells could be observed. Then, each clone was subcultured in larger well plates.

The cells were harvested for further detection. Genomic DNA was extracted with a Genomic DNA Extract Kit (Tiangen, Beijing, China) and amplified for mismatch enzyme identification and sequencing. The tPA primers for PCR were as follows: forward: 5′-GAAGCATCTTGGTTCGCTGC-3′, reverse: 5′-GGAGGCACAGAAGTTTCGCT-3′. The protein expression of tPA was detected by Western blot analysis.

2.3. Cell viability assay

3-(4,5-Dimethyl-2-thiazolyl)-2,5-diphenyl-2H-tetrazolium bromide (MTT) reagent (Merck, Darmstadt, Germany) was used to perform cell viability assays according to the manufacturer's protocol. Briefly, cells were plated in triplicate in 96-well plates at a density of approximately 2000 cells per well. The ischemia time was 4 h, 6 h or 8 h, with a reperfusion time of 3 h, 6 h, 12 h or 24 h for every ischemia time point. At the end of reperfusion, MTT solution was added to each well to a final concentration of 0.5 mg/mL, and the cells were incubated at 37 °C for 4 h. After discarding all the liquids gently, DMSO was added, and the cell culture plates were placed on a horizontal shaker to dissolve the crystals. The absorbance of each well was measured at 570 nm with a multimode microplate reader (SpectraMax 190, Molecular Devices, USA) immediately after the crystals were completely dissolved.

2.4. Western blot assay for protein expression

Total proteins were extracted using RIPA reagent supplemented with phenylmethylsulfonyl fluoride (PMSF) and phosphatase inhibitor (Solarbio, Beijing, China), while mitochondrial and cytoplasmic proteins were extracted using a commercial mitochondria isolation kit (Thermo Fisher, MA, USA). The bicinchoninic acid (BCA) (Beyotime, Beijing, China) method was used to quantify the protein concentration. Then, the proteins were electrophoresed using the SDS-PAGE technique. Briefly, after electrophoresis, the strips of gel containing the target proteins were cut, and the proteins were transferred to PVDF membranes depending on the molecular weight of the protein marker. The PVDF membranes were placed in 5% nonfat milk and blocked at room temperature for 2 h. After incubation with primary antibodies overnight at 4 °C followed by incubation with secondary antibodies for 2 h at room temperature, the PVDF membranes were scanned, and protein expression was analyzed with a gel imaging system (Fusion FX7, ViIbertLourmat, France). The following primary antibodies were used: anti-tPA, anti-Bax, anti-Bcl2, anti-Caspase9, anti-Cytochrome C (CytC), anti-COXIV (Proteintech, Rosemont, USA, 1:1000 dilution), anti-FUNDC1 (Abgent, Suzhou, China, 1:1000 dilution), anti-cleaved caspase3, anti-TOM20, anti-DRP1, anti-Parkin, anti-p-AMPK Thr172, anti-AMPK (Cell Signaling Technology (CST), MA, USA, 1:1000 dilution), anti-GAPDH, anti-mouse and anti-rabbit horseradish peroxidase-conjugated secondary antibodies (Proteintech, Rosemont, USA, 1:10000 dilution) were used.

2.5. Determination of the activity of Caspase3 and Caspase9

Caspase3 and Caspase9 activity was determined using Caspase3 and Caspase9 Activity Assay Kits (Beyotime, Beijing, China), respectively, according to the manufacturer's protocol. Briefly, cells digested with trypsin were collected in the corresponding medium, and the cell precipitate was obtained by centrifugation. After discarding the supernatant, the cells were washed with PBS and reprecipitated by centrifugation. Then, the precipitate was lysed, and the lysate was collected. After adding the detection agents and incubating the samples at 37 °C for 2 h, the absorbance at 405 nm was determined. The Bradford method was used to detect the protein concentration. The activity of Caspase3 or Caspase9 in each group was calculated according to the standard curve and protein concentration.

2.6. Detection of the apoptosis rate by flow cytometry

The apoptosis rate was determined using a Dead Cell Apoptosis Kit with Annexin V-FITC and PI for flow cytometry (Thermo Fisher, MA, USA). According to the protocol, cells were collected from each group and centrifuged after trypsin digestion to obtain the cell precipitate. The cells were precipitated twice with PBS, resuspended in binding buffer and mixed with 5 μL of Annexin V-FITC and 1 μL of PI for 15 min at room temperature. The apoptosis rate of each group was determined by flow cytometry (FACSCanto II, BD, USA).

2.7. Detection of mitochondrial membrane potential ($\Delta\Psi m$)

A commercially available ΔΨm assay kit with JC-1 (Beyotime, Beijing, China) was used. According to the protocol, cells were digested with trypsin and suspended in 0.5 mL of cell culture medium. JC-1 staining solution was added, and the sample was inverted several times to mix. The cells were incubated at 37 °C for 20 min. After incubation, the cells were centrifuged at 600×*g* for 4 min to obtain the precipitate. Then, the precipitate was washed twice with JC-1 staining buffer, and the ΔΨm was measured using flow cytometry (FACSCanto II, BD, USA). For murine brain tissue, after MCAO for 24 h, the mitochondria were extracted, mixed with JC-1 solution and then scanned with a multimode microplate reader (iD5, Molecular Devices, USA).

2.8. ROS content detection

According to the protocol of a ROS Assay Kit (Beyotime, Beijing, China), a serum-free culture solution was used to prepare a DCFH-DA solution with a final concentration of 10 μM. Following IR injury, cells were collected from each group. The cells were suspended in the DCFH-DA solution and incubated at 37 °C for 20 min. The solution was mixed by inversion every 3–5 min so that the probe would fully contact the cells. The cells were washed three times with serum-free cell culture medium to fully remove the DCFH-DA, which did not enter the cells. The ROS content of each group of cells was measured using flow cytometry (FACSCanto II, BD, USA).

2.9. Laser confocal imaging

The Ad-HBmTur-Mito (Hanbio, Shanghai, China) and LC3-GFP plasmids were used to detect mitochondria and autophagy, respectively. Briefly, HT22 cells and $tPA^{-/-}$ HT22 cells were seeded onto cell culture imaging dishes (NEST, Jiangsu, China) and transfected with LC3-GFP plasmids 12 h later. After 8 h, the culture medium was changed, and Ad-HBmTur-Mito was added to the medium. IR injury was induced 48–72 h later. At the end of reperfusion, the cells were fixed with 4% paraformaldehyde and stained with DAPI. Laser confocal microscopy (FluoView 1200, Olympus, Japan) was used to observe mitochondria and autophagy.

To assess the colocalization of tPA expression and mitophagy in cells in ischemic brains, paraformaldehyde-fixed paraffin-embedded brain tissue slices were harvested 6 h after MCAO from different groups and incubated with an anti-tPA antibody (Proteintech, USA, 1:50 dilution). An anti-NeuN antibody (Abcam, USA, 1:50 dilution) was used to identify neurons, and anti-LC3II (CST, USA, 1:400 dilution) and anti-TOM20 (Abcam, USA, 1:400 dilution) antibodies were used to identify mitophagy. Colocalization of tPA and mitophagy in neurons was detected by laser confocal microscopy (LSM 800, Zeiss, Germany).

2.10. Animals and middle cerebral artery occlusion (MCAO) model establishment

$tPA^{-/-}$ mice on the C57BL/6 background were purchased from the Jackson Laboratory (JAX; Bar Harbor, ME, USA). Wild-type (WT) and $tPA^{-/-}$ mice were maintained with food in a temperature-controlled animal room under a 12/12 h light/dark cycle for 2 weeks to adapt to the environment. A transient MCAO model was established following previously established methods [15]. Briefly, mice were anesthetized with 10% chloral hydrate. After skin preparation and disinfection, an incision was made in the cervical skin, and the external carotid artery was separated. A silk suture was advanced from the external carotid artery into the internal carotid artery until the origin of the middle cerebral artery. In the sham group, only external carotid artery separation was performed; no suture was placed. The skull of each mouse was exposed before the operation and connected to a laser Doppler flow meter (PF5001, Perimed, Switzerland). Animals with a cerebral blood flow decrease of more than 70% were considered successfully established MCAO models. The suture was withdrawn after 1 h of cerebral ischemia, which was followed by 24 h of reperfusion. The Doppler flow meter was used to monitor cerebral blood flow throughout the surgical process and cerebral reperfusion. All animal experiments were performed according to the guidelines of institutional animal care and use committees.

2.11. Neurological behavioral score assessment

Neurological deficits in mice were evaluated using the Modified Neurological Severity Score (mNSS), which includes motor, sensory, beam balance and reflex/abnormal movement measurements. The total possible score is 18 points, and higher scores indicate greater damage. The mNSS scores for the mice in each group were obtained 24 h after

ischemic treatment.

2.12. 2,3,5-Triphenyl-tetrazolium chloride (TTC) staining

To determine the infarct volume, mice were anesthetized with 10% chloral hydrate and sacrificed by decapitation 24 h after MCAO. After being completely excised and immediately placed in a −20 °C freezer for 20 min, the brains were cut into 2 mm thick slices and incubated in a 2% TTC (Merck, Darmstadt, Germany) solution at 37 °C for 15–30 min. The infarct volume was then calculated.

2.13. Real-time PCR

Total RNA was extracted from injured cerebral hemispheres or cells using TRIzol Reagent (Thermo Fisher, MA, USA) according to the manufacturer's instructions and reverse-transcribed into cDNA. The real-time fluorescence quantitative PCR method was used to amplify the target genes Bax, Bcl2, Caspase3, FUNDC1 and GAPDH using a SYBR Green qPCR kit (Roche, Basel, Switzerland). GAPDH was used as an internal reference. The total volume of the PCR system was 20 μL, including 2 μL of cDNA, 1 μL each of upstream and downstream primers, 10 μL of SYBR Green qPCR reagent, and 6 μL of ddH_2O. The reaction conditions were as follows: preheating at 95 °C for 5 min, denaturation at 95 °C for 15 s, and annealing and elongation at 60 °C for 30 s. Forty cycles were carried out. The relative expression of each target gene was calculated using the $2^{-\Delta\Delta CT}$ method. The following primers were used:

Bax forward: 5′-GACACCTGAGCTGACCTT-3′, reverse: 5′-CAGTTGAAGTTGCCATCAG-3′

Bcl2 forward: 5′-AAACCCTGTGCTGCTATC-3′, reverse: 5′-CTGTGTTCTTCATCGTTACTTC-3′

Caspase3 forward: 5′-CTGATGAGGAGATGGCTTG-3′, reverse: 5′-ACCCGTCCTTTGAATTTCT-3′

FUNDC1 forward: 5′-TGTGATATCCAGCGGCTTCG-3′, reverse: 5′-GCCGGCTGTTCCTTACTTTG-3′

GAPDH forward: 5′-TTCACCACCATGGAGAAGGC-3′, reverse: 5′-GGCATGGACTGTGGTCATGA-3′

2.14. TUNEL assay

After fixation, dehydration and paraffin embedding, brains were cut into 3 mm slices and baked at 72 °C for 1 h. After dewaxing and hydration in xylene, the antigens were repaired by high pressure. After incubation with 3% hydrogen peroxide, the slices were incubated with an anti-NeuN antibody (Abcam, USA, 1:100 dilution) at 4 °C overnight and then with goat anti-mouse Alexa Fluor 594 (Thermo Fisher, USA, 1:500 dilution) for 1 h at room temperature. Each slice was added to 50 μL of TUNEL detection solution (Beyotime, Beijing, China) and incubated at 37 °C for 1 h in the dark. After the nuclei were stained with DAPI, the slices were observed using laser confocal microscopy (LSM 800, Zeiss, Germany).

2.15. Transmission electron microscopy (TEM)

After MCAO for 6 h, mice were euthanized by choral hydrate administration and rapidly perfused with precooled PBS. The brains were then separated, and the ischemic cerebral cortex was cut into 1 mm^3 pieces and fixed in 2% glutaraldehyde. For the in vitro experiment, the cells were harvested at the end of IR injury. After washing with PBS, the cell precipitate was fixed in 2% glutaraldehyde. After sectioning and uranium lead double staining, the samples were observed and photographed with a TEM system (HT7800, Hitachi, Japan).

2.16. ATP content detection

A commercial ATP content detection kit (Beyotime, Beijing, China) was used. First, the culture medium was discarded, and 200 μL of lysis buffer was added to each well of a 6-well plate. The lysis buffer was aspirated repeatedly with a pipette to ensure that it fully contacted and lysed the cells. For brain tissue, 800 μL of lysis buffer was used, and the brain tissue was homogenized 24 h after MCAO with a glass homogenizer. Then, after complete lysis, the supernatant was harvested by centrifugation at 12000×*g* for 5 min at 4 °C. According to the manufacturer's instructions for the kit, a standard curve was drawn, and the ATP concentration of each group was measured. A BCA protein concentration kit was used to determine the protein concentration. The ATP content in each group was calculated.

2.17. Lactate dehydrogenase (LDH) release detection

According to the protocol of a LDH Detection Kit (Beyotime, Beijing, China), cell culture medium was collected from each group immediately after the end of reperfusion. After adding the detection solution and incubating the sample at room temperature for 30 min, the absorbance at 490 nm was measured with a multimode microplate reader to analyze the release of LDH release.

2.18. Bioinformatics analysis

A protein-protein interaction (PPI) network was constructed with the STRING database, and the interactive relationship among apoptosis, mitochondria and autophagy in the network was calculated and visualized with Cytoscape software. The related signaling pathways were then analyzed based on the Kyoto Encyclopedia of Genes and Genomes (KEGG) database.

2.19. Cell transfection

To observe the function of FUNDC1, the GV102-U6-shFUNDC1-SV40-Neomycin and GV146-CMV-FUNDC1-SV40-Neomycin plasmids were produced to knock down and overexpress FUNDC1 (GeneChem, Shanghai, China), respectively. According to the manufacturer's instructions for Lipofectamine 3000 (Thermo Fisher, MA, USA), the FUNDC1 knockdown and overexpression plasmids were transfected into $tPA^{-/-}$ HT22 cells. After transfection in Opti-MEM for 8 h, the cells were refreshed with normal medium.

2.20. Statistical analysis

SPSS17.0 statistical software was used to process the data. The data are presented as the mean ± SD. One-way ANOVA with a post hoc test was applied for multigroup comparisons. $P < 0.05$ was considered to indicate statistical significance.

3. Results

3.1. Knockout of tPA via CRISPR/Cas9 inhibited neuron viability in vitro

CRISPR/Cas9 technology, which can target individual genes, has proven to be a useful gene-editing tool for induction of transcription-level changes. To examine the roles of tPA, a stable $tPA^{-/-}$ HT22 hippocampal cell line was constructed by targeting a site on exon 4 (Fig. 1A). After infected with lentivirus-Cas9 and subjected to puromycin screening for 1–2 weeks, HT22 cells were also infected with lentivirus-sgRNA. Proteins were isolated from the cells for Western blot assessment of the knockout efficiency, which showed that tPA expression was significantly inhibited (Fig. 1B). The editing of the tPA gene was verified by sequencing (Supplementary Fig. 1). To further investigate whether tPA knockout could inhibit cell viability, we examined the cell viability in response to a range of durations of ischemia (4–8 h) and reperfusion (3–24 h). The results showed that the viability of $tPA^{-/-}$ HT22 cells was significantly lower than that of control HT22 cells at each IR time point (Fig. 1C–E).

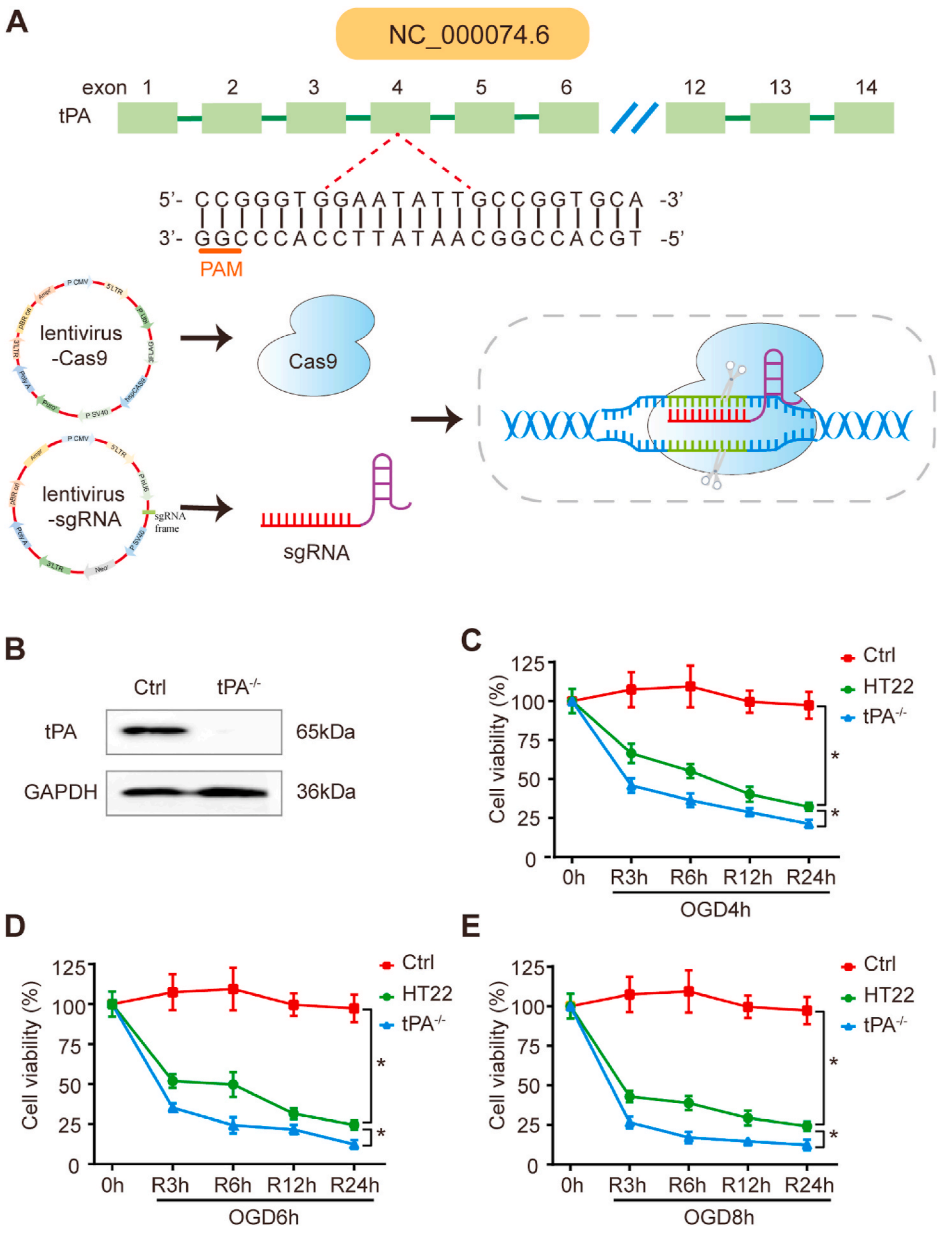

Fig. 1. tPA knockout by CRISPR/Cas9 inhibits neuronal viability in vitro. **(A)** Schematic protocol for CRISPR/Cas9 gene editing. (**B)** Western blot analysis was used to confirm the successful knockout of tPA. **(C–E)** Cell viability of WT and tPA$^{-/-}$ HT22 cells after different IR durations (mean ± SD, n = 3). Statistical comparisons were performed with one-way ANOVA. *$P < 0.05$.

3.2. tPA blocked the mitochondrial apoptosis pathway to protect against IR injury in vitro

To verify whether tPA has a protective role in neurons, we used the ischemia for 4 h followed by reperfusion for 3 h (I4hR3h) conditions in follow-up in vitro studies (see Fig. 2A for a schematic). First, we used western blotting to measure the protein expression of Bax, Bcl2, Caspase9 and Caspase3. We found that IR enhanced the expression of the proapoptotic proteins Bax, Caspase9, and Caspase3 and reduced the expression of the antiapoptotic protein Bcl2; tPA deficiency exacerbated these changes, but within the tPA$^{-/-}$ condition, tPA treatment reversed these changes (Fig. 2B–F). The patterns of activity for Caspase3 and Caspase9 were consistent with the protein levels observed by Western blot analysis (Fig. 2G and H). Then, cells were subjected to annexin V-FITC/PI-PE double staining to measure the apoptosis rate using flow cytometry. As shown in Fig. 2I, IR increased the apoptosis rate, and tPA$^{-/-}$ cells had a higher apoptosis rate than WT cells. The apoptosis rate in tPA$^{-/-}$ cells was dramatically decreased by the addition of tPA. We also conducted a preliminary study in brain microvascular endothelial cells (bEnd.3), and the antiapoptotic effect was also achieved in this cell line (Supplementary Fig. 2). Collectively, these results indicate that tPA blocks apoptosis induced by IR injury.

3.3. tPA reduced IR damage by improving mitochondrial function in vitro

Because mitochondrial injury is a critical contributor to IR injury and because the above research suggests that tPA suppresses the mitochondrial apoptosis pathway, our next set of analyses examined whether the antiapoptotic effect of tPA was accompanied by improved mitochondrial function. As JC-1 dye can be used to assess ΔΨm and ROS are the major products of IR damage, we used JC-1 and ROS assay kits to assess mitochondrial function. The results showed that cells with monomeric JC-1 (indicating depolarization) (Fig. 3A and B) and ROS production (Fig. 3C) increased following IR injury. Evidence of damage was greater

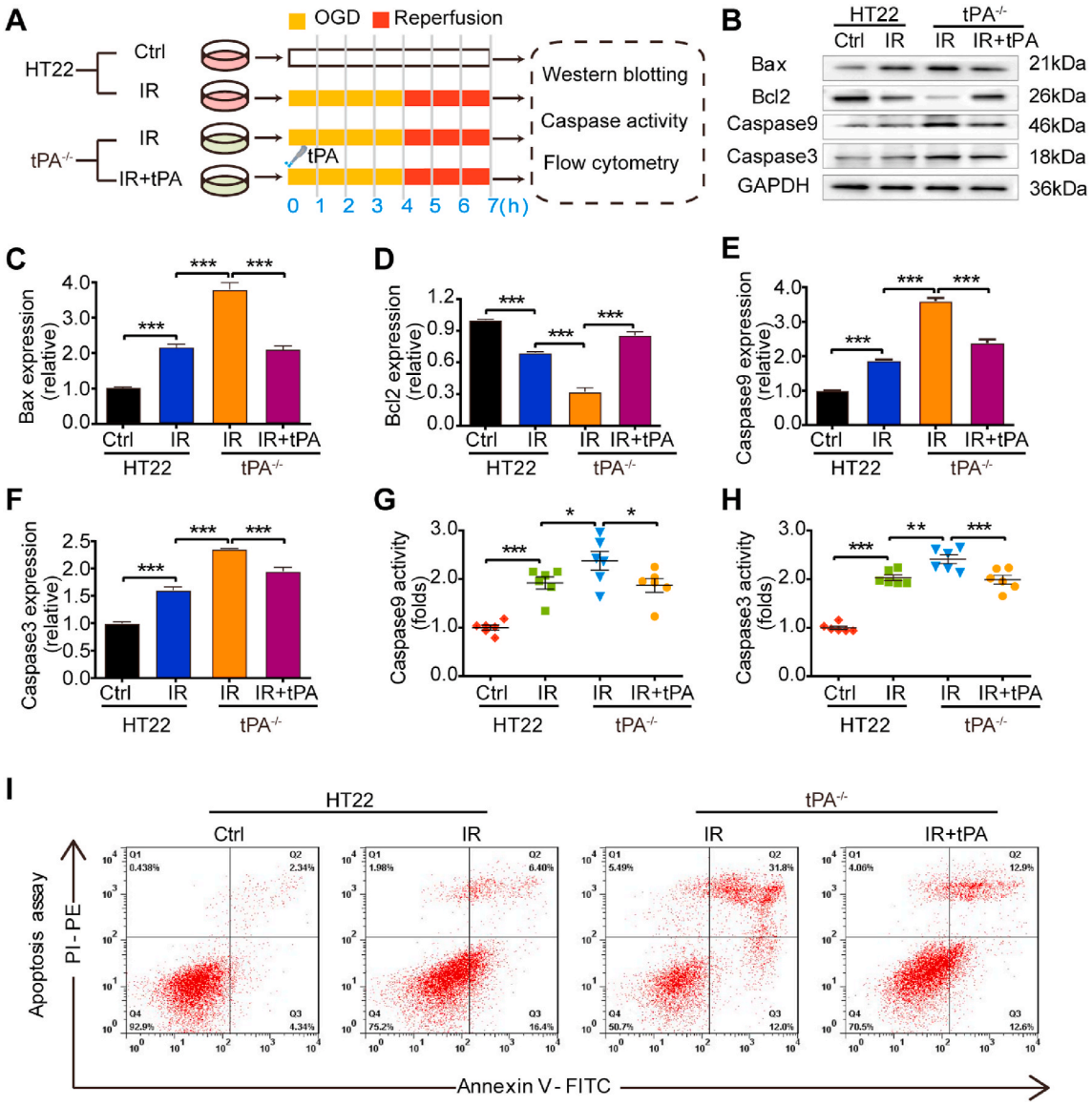

Fig. 2. tPA inhibits apoptosis in IR-injured HT22 cells. **(A)** Schematic protocol of the experiment. HT22 and tPA$^{-/-}$ HT22 cells were subjected to 4 h of OGD plus 3 h of reperfusion. In the IR + tPA condition, tPA was added at the beginning of OGD. **(B–F)** Western blotting was used to analyze the expression levels of the apoptosis proteins Bax, Bcl2, Caspase9 and Caspase3 at the end of reperfusion (mean ± SD, n = 3). **(G–H)** Caspase9 and Caspase3 activity was measured at the end of reperfusion (mean ± SD, n = 6). **(I)** The apoptosis rate was measured using flow cytometry at the end of reperfusion. Representative images from 3 independent experiments are shown. Statistical comparisons were performed with one-way ANOVA. *$P < 0.05$, **$P < 0.01$, ***$P < 0.001$.

in the tPA$^{-/-}$ condition. However, after addition of tPA, the ΔΨm stabilized, and ROS overproduction was alleviated (Fig. 3A–C).

Because mitochondrial apoptosis is closely associated with morphological changes, we next assessed evidence for mitochondrial fragmentation across cell conditions. As shown in Fig. 3D, IR led to mitochondrial fragmentation, which was greater in the tPA$^{-/-}$ condition than in the WT condition but could be reduced by tPA treatment. With mitochondrial fragmentation, the permeability of mitochondria increases, and CytC is released from the mitochondria into the cytoplasm, which activates caspase9. As shown in Fig. 3E–G, CytC leakage from mitochondria to the cytoplasm occurred after IR injury, and tPA deficiency promoted CytC release, which was limited by addition of tPA.

Finally, we assessed the levels of TOM20 and COXIV, two major mitochondrial proteins. We found that IR injury significantly decreased the levels of TOM20 and COXIV; the expression levels of both proteins were even lower in the tPA$^{-/-}$ condition than in the WT condition, but this difference was attenuated by addition of tPA (Fig. 3H–J). Taken together, these findings provide convergent evidence that tPA is important for protection of mitochondrial function during IR injury.

3.4. tPA decreased cerebral damage and apoptosis following IR in vivo

To investigate whether tPA has the same protective role in vivo, WT and tPA$^{-/-}$ mice were subjected to transient MCAO for 1 h followed by reperfusion for 24 h (see Fig. 4A for schematic). First, neurological deficit scores and infarct volumes were measured. The results showed that following IR injury, tPA$^{-/-}$ mice had higher neurological deficit scores and larger cerebral infarct volumes than WT mice. There were no significant differences between the WT sham and tPA$^{-/-}$ sham groups (Fig. 4B–D). We next measured the effect of tPA on cerebral apoptosis. We used Western blot analysis and real-time PCR to measure the protein and mRNA levels, respectively, of important mitochondria-related apoptosis factors, including Bax, Caspase3 and Bcl2. IR injury was associated with increased expression of Bax and Caspase3 and reduced expression of Bcl2 in the WT mice. Additionally, tPA$^{-/-}$ mice showed higher Bax and Caspase3 expression and lower Bcl2 expression than WT

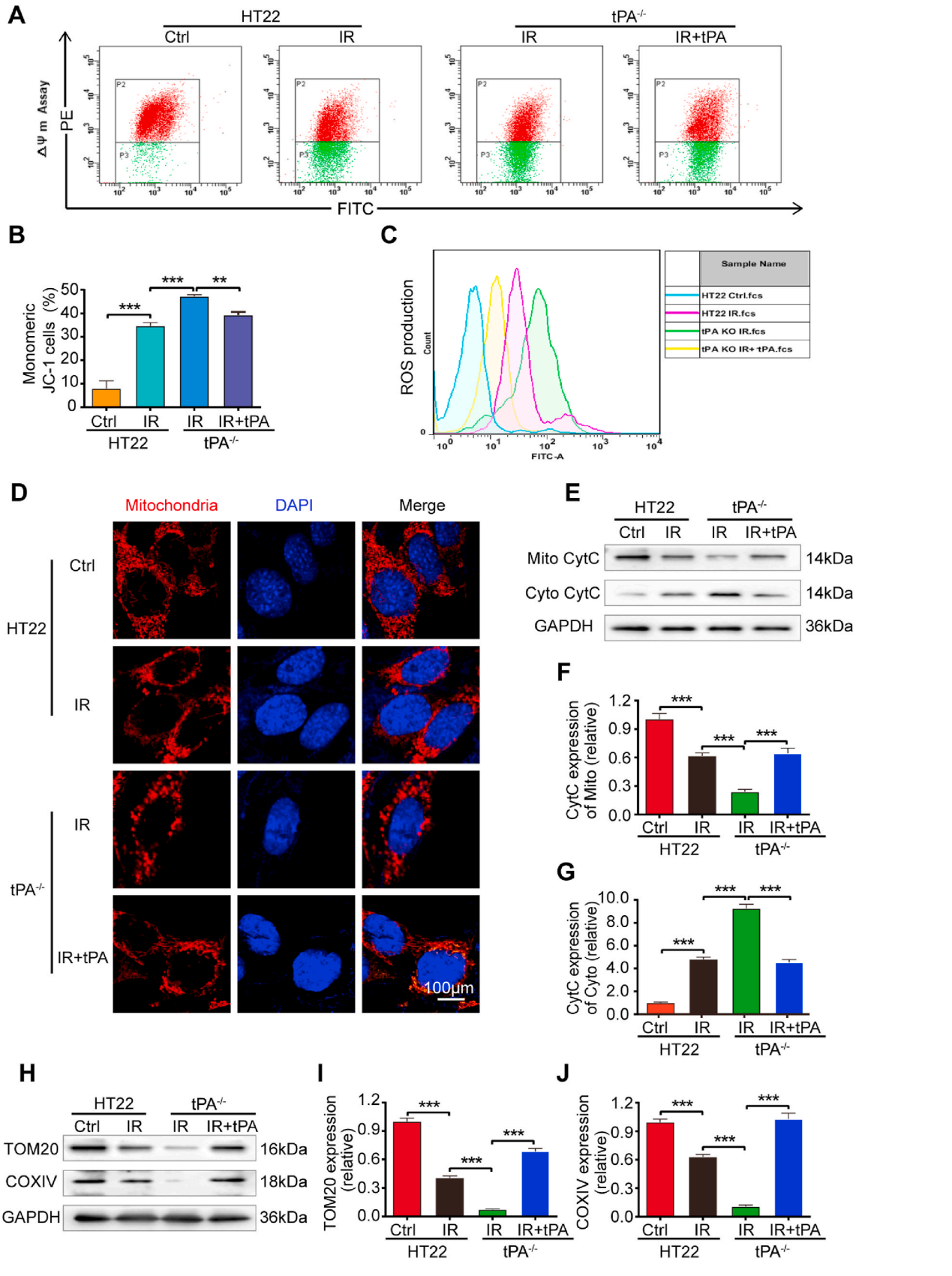

(caption on next page)

Fig. 3. tPA protects mitochondria from IR injury. **(A)** Mitochondrial health was assessed using JC-1 staining in a ΔΨm assay. Within each chart, cells with monomeric JC-1 in the P3 region are shown in green and represent damaged mitochondria, while cells with polymeric JC-1 in the P2 region are shown in red and represent healthy mitochondria. Representative images from 3 independent experiments are shown. **(B)** Quantification of the results of JC-1 staining, with the percentage of cells with monomeric JC-1 (representing cells with impaired mitochondrial function and apoptosis) in each condition shown (mean ± SD, n = 3). **(C)** ROS production was measured by flow cytometry in each condition. Representative images from 3 independent experiments are shown. **(D)** Fragmented mitochondria were observed in IR-injured cells by laser confocal microscopy. **(E–G)** Western blot analysis was used to detect CytC leakage from mitochondria to the cytoplasm. In normal cells, CytC was located in mitochondria. However, IR resulted in the diffusion of CytC from damaged mitochondria into the cytoplasm (mean ± SD, n = 3). **(H–J)** Western blot analysis was used to detect the protein expression levels of TOM20 and COXIV, two mitochondrial marker proteins (mean ± SD, n = 3). Statistical comparisons were performed with one-way ANOVA. $^{**}P < 0.01$, $^{***}P < 0.001$. (For interpretation of the references to colour in this figure legend, the reader is referred to the Web version of this article.)

mice (Fig. 4E–K). Next, to provide convergent evidence for the effects of tPA on neurons, an anti-NeuN antibody was used to mark neurons, and cerebral slices were colabeled in a TUNEL assay. As shown in Fig. 4L, elevated counts of TUNEL-positive neurons were associated with IR injury, and tPA deficiency increased the number of TUNEL-positive neurons after IR injury. There were no significant differences between the WT sham and $tPA^{-/-}$ sham groups.

Because Bax and Bcl2 are well-known apoptosis proteins related to mitochondria, we investigated mitochondrial alterations in IR mice through TEM. The results showed numerous dendrites and dense, intact mitochondrial structures (yellow arrow) in the brains of WT sham and $tPA^{-/-}$ sham mice. After IR, the brain tissue of WT mice was injured, the mitochondrial structure was damaged, and the cristae were disrupted. There was not only autophagy (purple arrow) but also widespread mitophagy (green arrow) in the WT IR mouse brains. In the brains of $tPA^{-/-}$ IR mice, the mitochondrial structure was disrupted, and mitochondrial vacuolation was obvious (Fig. 4M). Similarly, we found mitochondrial damage and changes in autophagy in the endothelial cells of IR-damaged mice (Supplementary Fig. 3). These results suggest that tPA affects the mitochondrial apoptosis pathway through mitophagy.

3.5. tPA affects mitochondrial function and apoptosis through mitophagy

Mitophagy, as a selective form of autophagy, plays an important role in maintaining mitochondrial function. In view of our current results that $tPA^{-/-}$ may inhibit mitochondrial function, we wanted to explore whether the protective effect of tPA on the mitochondrial pathway of apoptosis is related to mitophagy.

As DRP1 is a regulator of mitophagy, its mitochondrial translocation is closely related to mitochondrial fragmentation. Therefore, we first assessed the mitochondrial translocation of this protein. We found that the translocation of DRP1 to mitochondria increased during IR and that $tPA^{-/-}$ promoted this translocation; the effect of $tPA^{-/-}$ was reversed by addition of tPA (Fig. 5A–C). These findings suggest that mitophagy may be involved in the effect of tPA on apoptosis.

Then, TEM was used to observe the changes in mitochondrial structure and mitophagy. The results showed that in the HT22 WT group, the cell structure was clear, and the mitochondria were dense and complete. IR damage caused mitochondrial swelling and necrosis, and mitophagy was observed; however, in the $tPA^{-/-}$ HT22 cells, the organelles were difficult to distinguish, and mitochondrial cavitation was pronounced, but mitophagy was hardly visible. tPA alleviated mitochondrial damage, and increased mitophagy was observed in the subgroup of $tPA^{-/-}$ HT22 cells treated with tPA (Fig. 5D).

To further confirm the relationship among tPA, mitochondria, autophagy and apoptosis, 3-methyladenine (3MA) was used in our study. We transfected HT22 cells with LC3-GFP plasmids and Ad-HBmTur-Mito to observe the colocalization of autophagy and mitochondria. IR injury caused autophagy in HT22 cells, which was weaker in the $tPA^{-/-}$ condition. Within $tPA^{-/-}$ cells, tPA treatment increased mitophagy, and further introduction of 3MA successfully blocked mitophagy (Fig. 5E).

Next, we measured factors associated with mitochondria, cell damage, and apoptosis, including ATP content, LDH release, and apoptosis protein (Bax, Caspase3, and Bcl2) expression. As shown in Fig. 5F and G, ATP content decreased and LDH release increased after IR injury, and these effects were stronger in $tPA^{-/-}$ cells than in WT cells. In $tPA^{-/-}$ cells, tPA treatment increased ATP content and reduced LDH release, and these effects were blocked by addition of 3MA. A corresponding pattern of results was found for the apoptosis proteins. As with other measures, $tPA^{-/-}$ cells showed exacerbated effects that were ameliorated by tPA treatment, and this amelioration was in turn reversed by 3MA treatment (Fig. 5H–K). These findings suggest that tPA affects mitophagy, which impacts mitochondrial function and apoptosis.

3.6. tPA influenced mitochondrial function and neuronal mitophagy

To further confirm that tPA affects mitophagy and mitochondrial function, we performed a series of in vivo experiments. Our results showed that $tPA^{-/-}$ further decreased the ΔΨm and ATP content after cerebral IR damage but did not cause significant changes in the WT sham and $tPA^{-/-}$ sham groups, which suggests that tPA plays a more important role under conditions of ischemic injury than under normal physiological conditions (Fig. 6A and B).

Exposure to hypoxia has previously been shown to induce rapid release of tPA from neurons but not from astrocytes in order to promote cell survival [14]. Thus, we next identified the types of cells showing mitophagy in ischemic brains and examined the colocalization of tPA expression and mitophagy in ischemic brains using biomarkers. IR injury decreased tPA expression in neurons and promoted colocalization between LC3II and mitochondria in WT mice, while this colocalization was suppressed in $tPA^{-/-}$ mice, suggesting that tPA induces mitophagy (Fig. 6C).

3.7. Identification of FUNDC1 as a bridge linking tPA-regulated apoptosis and mitophagy during IR damage

The above results suggested that mitophagy plays a pivotal role in tPA-regulated apoptosis, but how mitophagy is involved in tPA regulation remained unclear. We detected the protein levels of parkin, a marker of mitophagy, in IR-injured HT22 cells. We found that parkin protein levels increased after IR but that tPA had no relationship with Parkin (Fig. 7A and B). This finding suggests that tPA may affect mitophagy through other mechanisms.

Therefore, we searched the STRING database and drew an interaction network including FUNDC1, mitophagy and apoptosis. The PPI network suggested that FUNDC1 may be a key bridge between apoptosis and mitophagy (Fig. 7C). Analysis of the related signal pathways suggested that the proteins are involved in different signaling pathways (Fig. 7D).

To test the hypothesis that FUNDC1 acts as a bridge, we measured differences in FUNDC1 mRNA levels and protein expressions under different conditions in vivo and in vitro (see Fig. 7E for schematic). The results showed that both in the brains of mice (in vivo) and in HT22 cells (in vitro), the mRNA expression of FUNDC1 in the WT group was lower after IR than under control conditions, and the IR-induced decrease was greater in the $tPA^{-/-}$ group than in the WT group. The effect of tPA knockout was reduced by introduction of tPA in vitro (Fig. 7F and G). In related analyses, we measured the protein expression of FUNDC1 and found similar effects of IR and tPA knockout in vivo and in vitro and

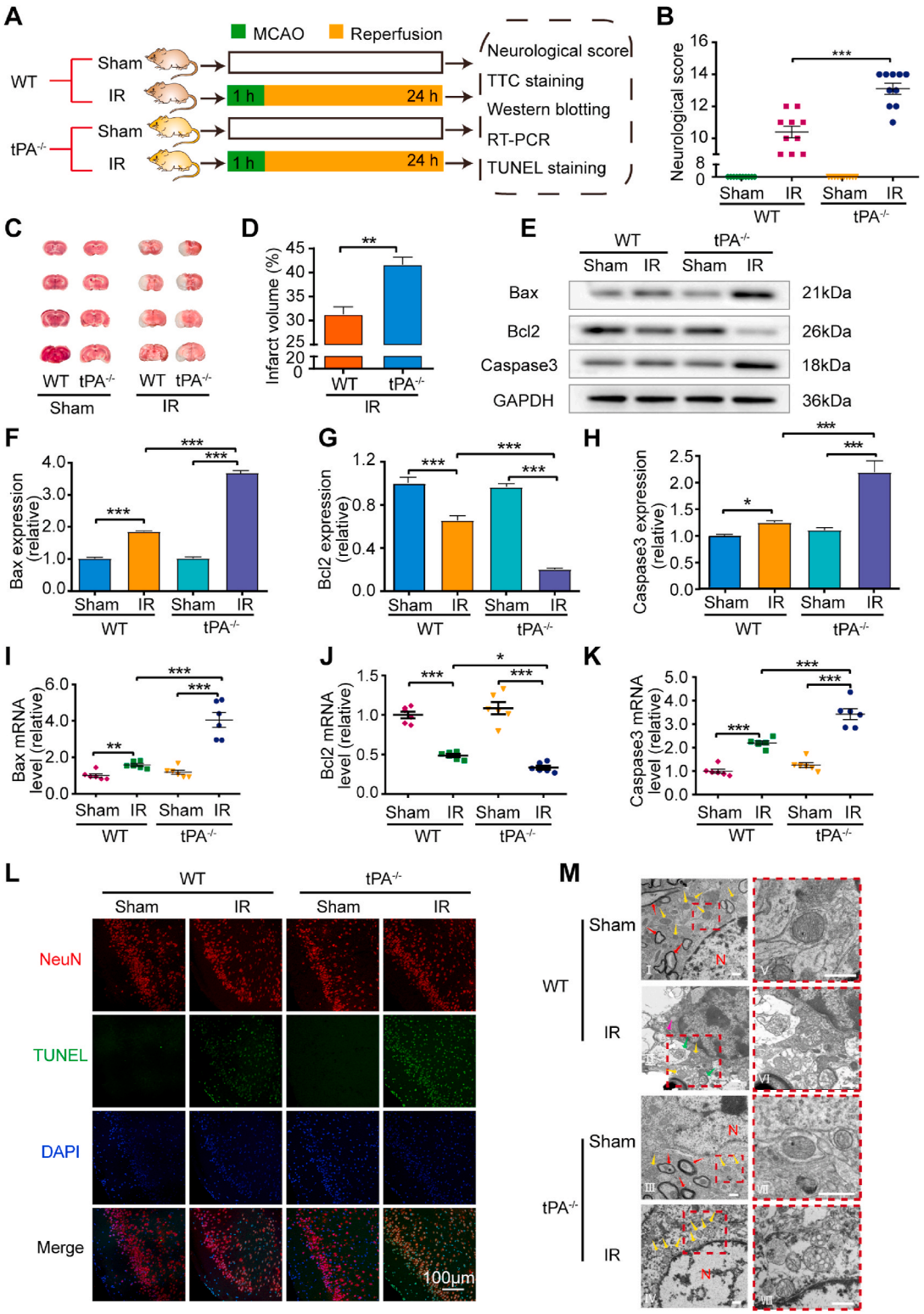

Fig. 4. tPA protects against cerebral damage following IR injury. **(A)** Schematic protocol of IR injury in vivo. Mice underwent 1 h of MCAO followed by 24 h of reperfusion. **(B)** mNSS scores (maximum of 18, where higher scores indicate greater deficits) of mice measured 24 h after reperfusion (mean ± SD, n = 10). **(C-D)** The infarct volume was determined by TTC staining. Representative TTC-stained brain slices from each group are shown. **(E–H)** Western blot analysis of the protein expression of Bax, Bcl2 and Caspase3 in the cerebral hemisphere with IR injury (mean ± SD, n = 3). **(I–K)** Real-time PCR (RT-PCR) was used to evaluate the mRNA levels of Bax, Bcl2 and Caspase3 in the cerebral hemisphere with injury (mean ± SD, n = 6). **(L)** TUNEL and NeuN costaining was performed to assess neuronal apoptosis and indicated that tPA knockout increased the number of TUNEL-positive neurons in the context of IR injury. Representative images from each group are shown. **(M)** Neuronal and mitochondrial structures were observed by TEM. Scale bar = 6 μm. The boxed regions in the left panels are enlarged in the right panels. Red arrow: axon; yellow arrow: mitochondria; purple arrow: autophagy; green arrow: mitophagy. Statistical comparisons were performed with one-way ANOVA. $^{*}P < 0.05$, $^{**}P < 0.01$, $^{***}P < 0.001$. (For interpretation of the references to colour in this figure legend, the reader is referred to the Web version of this article.)

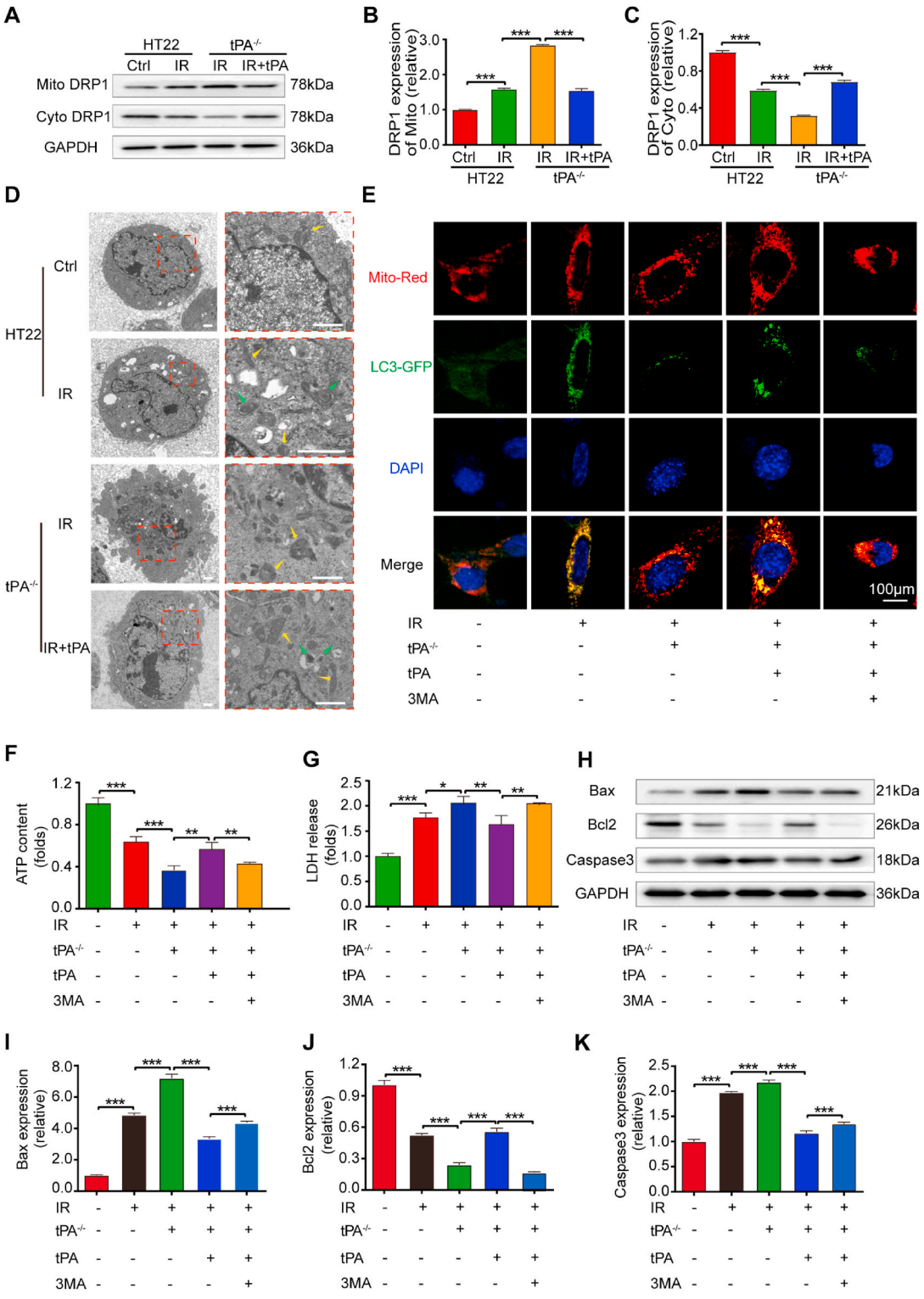

Fig. 5. tPA affects mitochondrial apoptosis and function by activating mitophagy. **(A–C)** Western blot analysis was used to measure the translocation of DRP1 to mitochondria. IR injury increased the translocation of DRP1 to mitochondria. tPA knockout augmented this translocation, but the augmentation was reversed by tPA addition (mean ± SD, n = 3). **(D)** The mitochondrial structures of HT22 cells were observed by TEM. Scale bar = 10 μm. **(E)** Laser confocal microscopy was used to observe mitophagy. IR injury increased autophagy and increased its colocalization with mitochondria in HT22 cells, but these effects were weakened by tPA knockout. Exogenous tPA enhanced mitophagy, which could be blocked by 3MA. Representative images from each group are shown. Scale bar = 100 μm. **(F–G)** ATP content and LDH release. ATP content decreased and LDH release increased after IR injury in the control condition; these effects were magnified in the $tPA^{-/-}$ condition. Exogenous tPA increased ATP content and reduced LDH release, and these effects were reversed by addition of 3MA (mean ± SD, n = 4). **(H–K)** The expression levels of the apoptosis proteins Bax, Caspase3, and Bcl2 were measured by Western blot analysis (mean ± SD, n = 3). Statistical comparisons were performed with one-way ANOVA. $^{*}P < 0.05$, $^{**}P < 0.01$, $^{***}P < 0.001$.

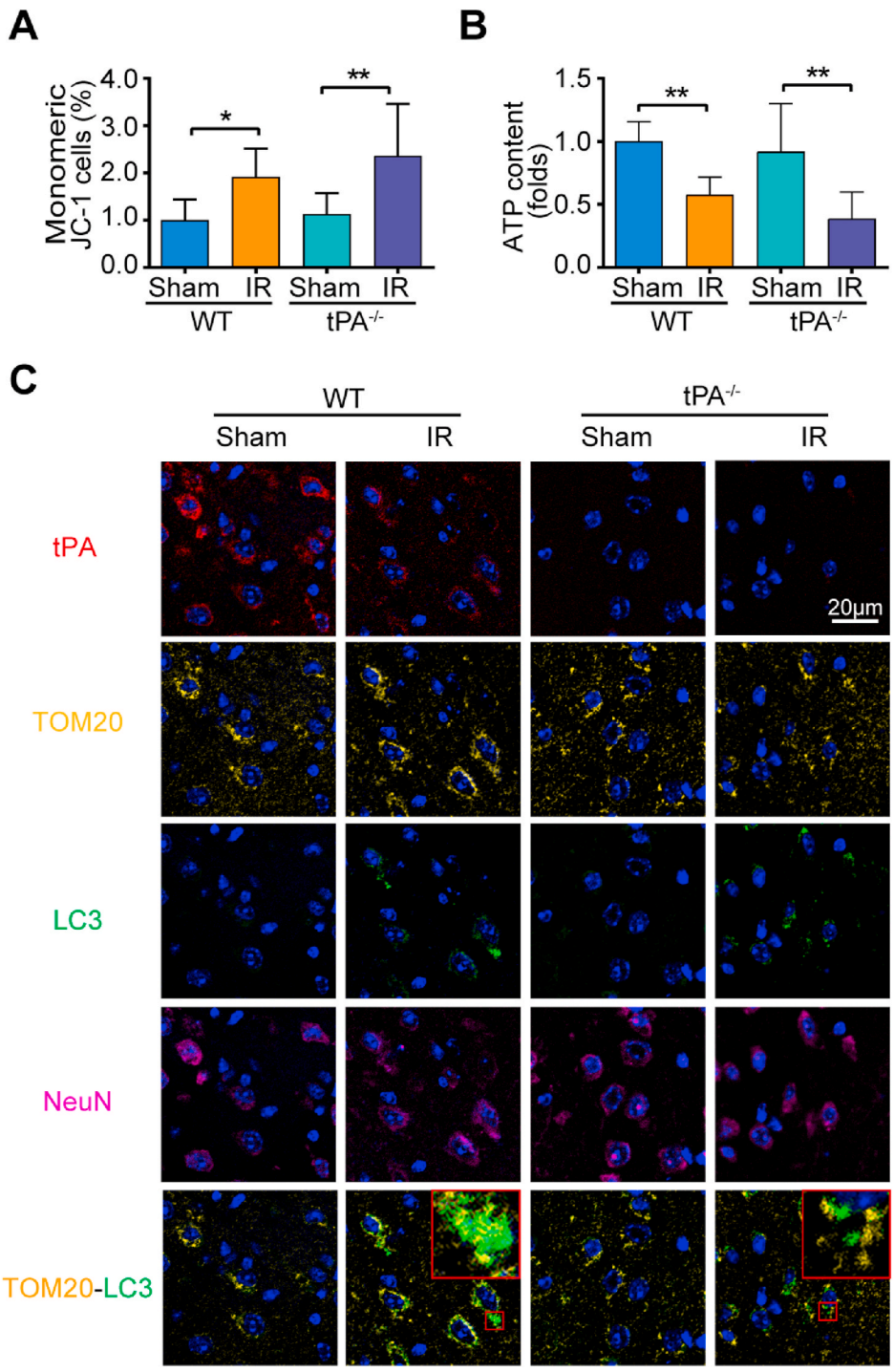

Fig. 6. tPA influences mitochondrial function and neuronal mitophagy. **(A–B)** ΔΨm and ATP content were measured in vivo. IR injury decreased the ΔΨm and ATP content. tPA knockout augmented these changes (mean ± SD, n = 3). **(C)** Colocalization of tPA and mitophagy in neurons. IR injury decreased tPA expression in neurons and promoted colocalization between LC3II and mitochondria in WT mice. This colocalization was suppressed by tPA knockout.Statistical comparisons were performed with one-way ANOVA. *$P < 0.05$, **$P < 0.01$.

similar effects of tPA treatment in vitro (Fig. 7H–K). These results suggest that tPA positively regulates FUNDC1 levels, which may, in turn, play an important mediating role in IR injury.

3.8. FUNDC1 mediates the activation of mitophagy by tPA, and AMPK phosphorylation participates in this process

FUNDC1 is a mitochondrial membrane protein with a three-transmembrane structure that has a cytosol-exposed LIR in the N-terminal region [10]. Studies have shown that FUNDC1 is related to mitophagy and is widely involved in the effects of IR, but whether it is related to tPA-induced mitophagy is unclear. In our next set of analyses, we wanted to examine whether FUNDC1-dependent mitophagy is related to the neuroprotective effect of tPA during IR; for this purpose, we knocked down or overexpressed FUNDC1 in tPA$^{-/-}$ HT22 cells (Supplementary Fig. 4). First, we knocked down FUNDC1 in tPA$^{-/-}$ HT22 cells and used western blotting to measure the interaction effect of tPA and FUNDC1 on apoptosis. The results showed that, as previously found, tPA introduction reduced Bax and Caspase3 expression and increased Bcl2 expression within tPA$^{-/-}$ cells. However, these patterns were reversed in the tPA$^{-/-}$ + tPA condition with FUNDC1 knockdown (the tPA$^{-/-}$+ tPA + sh-FUNDC1 condition) (Fig. 8A–D). These findings suggest that FUNDC1 mediates the antiapoptotic role of tPA. Next, we overexpressed FUNDC1 in tPA$^{-/-}$ HT22 cells to assess whether FUNDC1

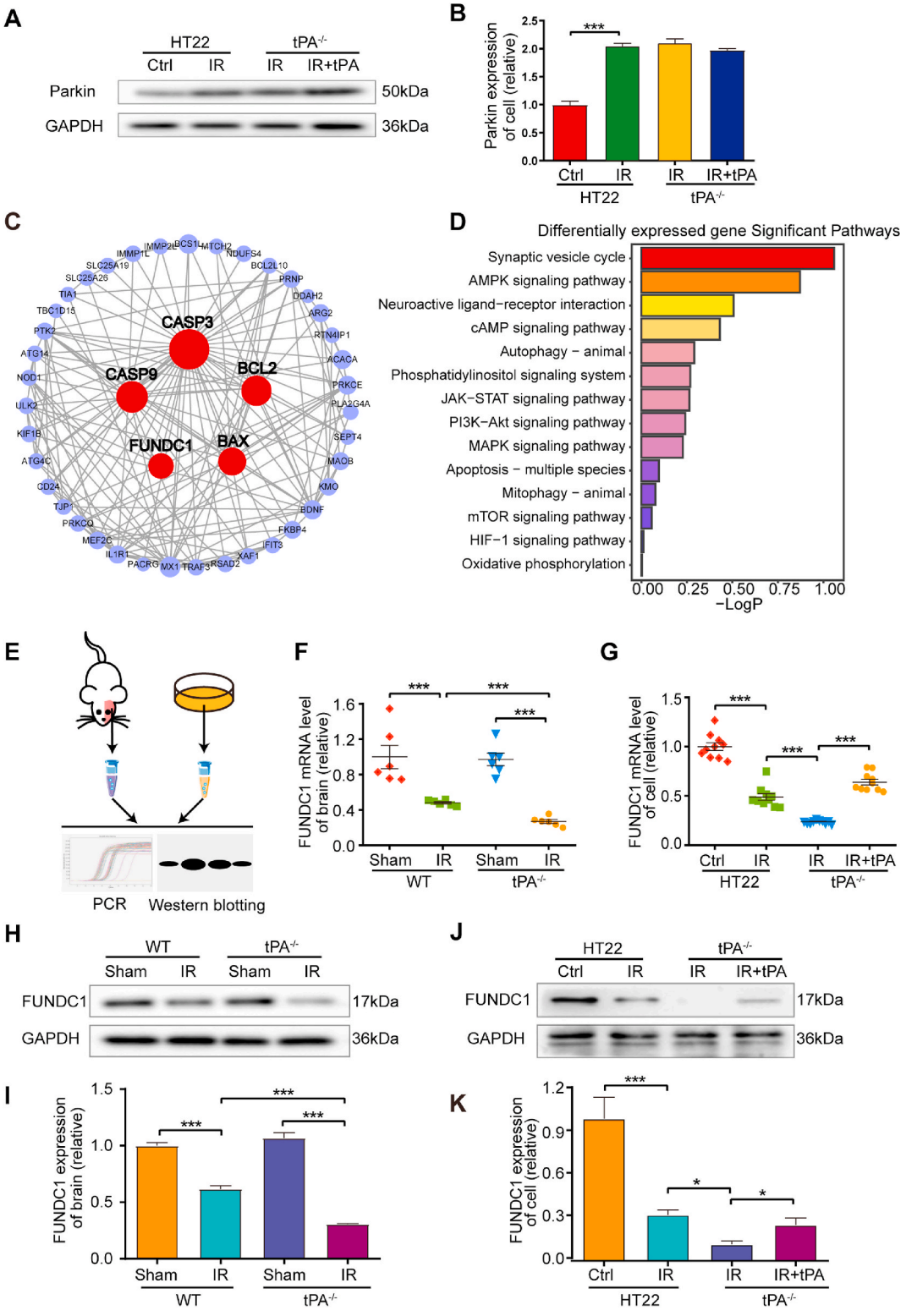

Fig. 7. Identification of FUNDC1 as a bridge linking tPA-regulated apoptosis and mitophagy in IR damage. **(A–B)** Parkin protein levels in IR-injured HT22 cells. The protein levels of parkin increased after IR, but tPA had no relationship with Parkin (mean ± SD, n = 3). **(C–D)** PPI analysis and KEGG analysis revealed an interaction network in which FUNDC1 may be at the core of autophagy, mitochondrial and apoptosis along with their related signaling pathways. **(E)** Schematic protocol for FUNDC1 measurement. **(F–G)** FUNDC1 mRNA level in each condition in vivo and in vitro (mean ± SD, n = 6 in vivo and n = 10 in vitro). **(H–K)** The protein expression levels of FUNDC1 were measured in the injured cerebral hemisphere in vivo (H–I) and in vitro (J–K) (mean ± SD, n = 3). Statistical comparisons were performed with one-way ANOVA. $^{*}P < 0.05$, $^{***}P < 0.001$.

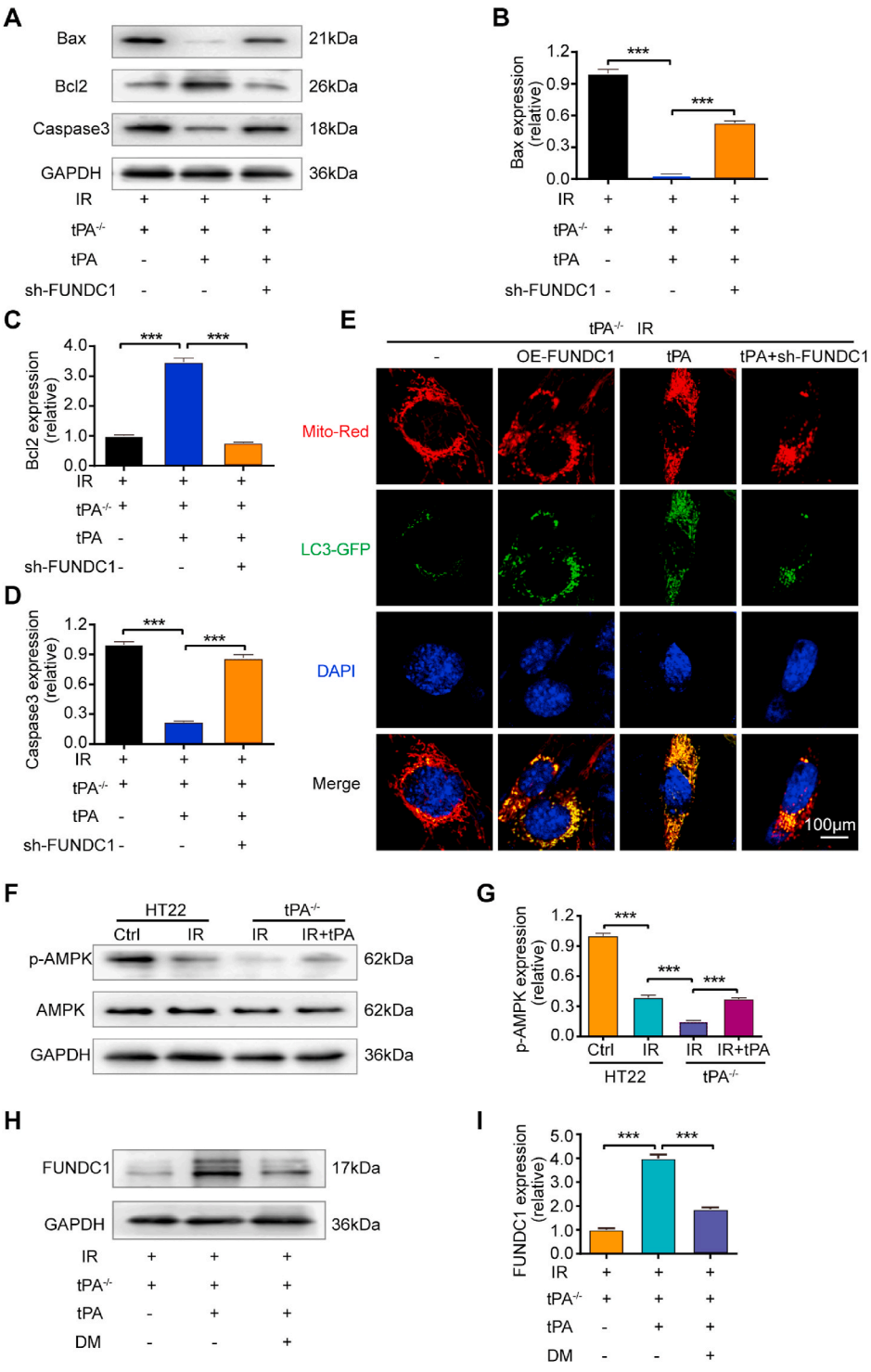

Fig. 8. tPA-related mitophagy is FUNDC1 dependent and triggered by AMPK phosphorylation. **(A–D)** Western blot analysis was used to measure the protein expression levels of Bax, Caspase 3 and Bcl2 following FUNDC1 knockdown. FUNDC1 knockdown altered tPA-induced Bax, Caspase3 and Bcl2 protein expression (mean ± SD, n = 3). **(E)** tPA-activated mitophagy is FUNDC1 dependent. OE-FUNDC1 increased the colocalization of autophagy and mitochondria, whereas FUNDC1 knockdown blocked the increase in mitophagy. Representative images from each group are shown. **(F–G)** The phosphorylation of AMPK was involved in IR damage and changed depending on the tPA level. The p-AMPK level was decreased following IR injury; the absence of tPA aggravated this change, and the effect of tPA knockout was reversed by addition of tPA (mean ± SD, n = 3). **(H–I)** The AMPK inhibitor DM reduced the effect of tPA on the expression of FUNDC1 (mean ± SD, n = 3). Statistical comparisons were performed with one-way ANOVA. ***$P < 0.001$.

mediated the activation of mitophagy by tPA. The results showed that FUNDC1 overexpression (OE-FUNDC1) increased the colocalization of LC3II and mitochondria in tPA$^{-/-}$ cells following IR injury. Additionally, in tPA$^{-/-}$ cells treated with tPA (tPA$^{-/-}$+ tPA), FUNDC1 knockdown blocked the increase in LC3II/mitochondrial colocalization (Fig. 8E). These complementary findings suggest that tPA-mediated mitophagy is dependent on FUNDC1.

Wu et al. [13] and An et al. [14] reported that neurons expressing tPA or neurons incubated with tPA exhibit continuous AMPK activation after IR, which enables the neurons to perceive and adapt to metabolic stress caused by IR damage, increases neuronal ATP synthesis, and protects neurons. Our results showed that 3MA-mediated inhibition of the protective effect of tPA affected ATP production (Fig. 5F), and bioinformatics analysis suggested that FUNDC1 and apoptosis-related proteins have an important relationship with the AMPK signaling pathway (Fig. 7D). Therefore, we hypothesized that the AMPK signaling pathway is involved in the tPA regulation process and in FUNDC1-mediated mitophagy regulated by tPA. In support of this hypothesis, p-AMPK levels decreased following IR and decreased to a greater extent in the tPA$^{-/-}$ group; in addition, the effect of tPA knockout was reversed by the addition of tPA (Fig. 8F and G). Next, we measured whether p-AMPK levels were related to tPA-induced FUNDC1 expression

by applying the AMPK inhibitor dorsomorphin (DM) to the $tPA^{-/-}$+ tPA condition. Surprisingly, although introduction of tPA to $tPA^{-/-}$ cells increased the expression of FUNDC1, further introduction of DM reduced FUNDC1 levels, indicating that the regulation of FUNDC1 by tPA was mediated by AMPK phosphorylation (Fig. 8H and I).

4. Discussion

This study intended to investigate the role of tPA in the response to IR and to explore the possible mechanisms. By using CRISPR/Cas9, the latest gene-editing technology, we explored the neuroprotective effects of endogenous tPA against cerebral IR injury. The results showed that knockout of tPA from neuronal cells decreased cell viability and increased apoptotic cell death. tPA treatment reversed neuronal cell damage in $tPA^{-/-}$ cells in vitro. This phenomenon was also confirmed in an in vivo study on $tPA^{-/-}$ mice. Furthermore, tPA was revealed to protect mitochondrial function, perhaps through modulation of the FUNDC1-dependent mitophagy pathway.

It is widely accepted that the neurotoxic or neuroprotective roles of tPA are related to the concentrations of tPA, the types of cells, the experimental models or combinations of these factors [6,16]. Most studies have reported that tPA is neurotoxic in the dose range of 20–500 μM, which is higher than the concentration of tPA in brain tissue under physiological and pathological conditions. Recently, we discovered that exogenous recombinant tPA (rtPA) at a dose of 9 mg/kg weight in vivo or 50 μg/mL in vitro exerts a neurotoxic effect by disrupting the blood-brain barrier through enhancement of the inflammatory response after cerebral ischemia [17]. Neurotoxic effects of rtPA have also been observed in studies performed by Wei et al. [18] and Kim et al. [19]. On the other hand, increasing evidence has recently revealed that endogenous release of tPA during the acute phase of ischemic injury may be a beneficial response aimed at protecting damaged neurons [2]. Compared to the neurotoxicity studies on rtPA, studies on the protective effects of rtPA have used lower doses of tPA that are closer to the actual level of tPA in the brain [6]. These studies have revealed that a physiological dose of tPA acts on various cellular receptors and exerts neuroprotective effects through a variety of cellular signaling pathways. For example, tPA can activate NMDA receptors in cortical neurons injured by IR and increase the expression levels of neuronal TNFα and phosphorylated Akt to induce neuron tolerance during early ischemia [15,20]. tPA can also activate the membrane protein AII and promote synaptic extension and neuronal survival through the ERK1/2-CREB-ATF3 [21], PKB and Akt [20] pathways. Other pathways, such as the mTOR-HIFα pathway, have also been implicated in the neuroprotective effects of tPA [22]. Wu et al. [13] found that the energy metabolism of neurons is disordered during IR and that tPA can improve glucose absorption in IR-injured neurons and promote ATP production to protect neurons. In these studies, the tPA dose was 5 nM or lower in vitro.

Mitochondria are the main targets of IR. Restoration of blood flow after ischemia induces oxidative stress in mitochondria, which can lead to mitochondrial dysfunction and promote the release of cytochrome and Bcl2 family members. The lack of nutrients and excitotoxic damage caused by IR itself are important inducers of neuronal autophagy. These changes stimulate the interaction of mitochondrial membrane receptors with LC3 to remove harmful mitochondria in a timely and effective manner, which helps to reduce oxidative stress damage, maintain energy and metabolic balance, and reduce IR damage. However, excessive autophagy induces programmed cell death. Autophagy/mitophagy can be elicited by ischemia, but the involvement of autophagy/mitophagy in the postischemic reperfusion phase helps determine the fate of neurons. The outcome of mitophagy in the context of IR may depend on the durations of the ischemia phase and the reperfusion phase [24]. Among mouse models of cerebral IR, most are induced by 1 h of MCAO plus 24 h of reperfusion [23,24]. This paradigm has also been used in many studies on tPA in neurons and in studies on IR-induced mitophagy. To study the effect of tPA on neuronal apoptosis, we subjected mice to 1 h of MCAO and measured the expression of apoptosis-related protein in the injured hemispheres after different durations of reperfusion, such as 6 h, 12 h and 24 h. The results showed that the protein levels of caspase3 increased with prolonged reperfusion time, as shown in Supplementary Fig. 5. Zhang et al. [24] and He et al. [25] established cerebral MCAO models with 1 h of ischemia plus 24 h of reperfusion in mice and rats, respectively. They discovered that suppression of mitophagy exacerbated neuronal injury, similar to our findings in the present study. In another MCAO model established by 6 h of ischemia plus 18 h of reperfusion, cerebral function was improved by inhibition of mitophagy [26]. These results indicate that the duration of ischemia has a substantial effect on mitophagy. More intriguingly, research on similar MCAO models (MCAO with 2 h of ischemia plus 22 h of reperfusion) has revealed that regulation of mitophagy before ischemia and regulation of mitophagy at the onset of reperfusion may produce contrasting results [27,28]. These findings indicate that reperfusion may be a key variable for the regulation of mitophagy in ischemic cerebral tissue.

In our previous study, we found that tPA can activate neuronal autophagy during IR injury. However, whether tPA can induce removal of damaged mitochondria by mitophagy has not been reported. To the best of our knowledge, we are the first to provide evidence that tPA protects neurons by activating mitophagy in order to reduce neuronal apoptosis. Upon mitochondrial stress, such as IR stress, bioenergetic stress and oxidative stress, receptors that are localized to the outer mitochondrial membrane undergo enhanced interaction with LC3 or other autophagy genes and initiate mitophagy. How mitophagy receptors sense these stresses to activate mitophagy remains largely unknown, but distinct mitophagy mechanisms are activated by different mitochondrial stresses [29]. FUNDC1 receptor-mediated mitophagy is the major mitophagy pathway in mammalian cells subjected to IR. Zhou et al. [30] found that cardiac IR injury significantly increases the levels of mitophagy and mitochondrial damage. The increase in mitophagy is caused by changes in the FUNDC1 phosphorylation level, which affects apoptosis. It has been suggested that FUNDC1 participates in IR-activated mitophagy and affects mitochondrial apoptosis. This idea is similar to our results. However, unlike the Zhou's study, our experiment revealed that FUNDC1 is involved in IR-induced mitophagy through changes in expression levels regulated by AMPK phosphorylation. It is possible that the different disease types have different mechanisms.

Wu et al. [31] found that mitochondrial dysfunction caused by high glucose is an important cause of diabetic heart disease. In this process, high glucose increases the levels of FUNDC1, resulting in mitochondrial dysfunction, and AMPK participates in this process. It has been suggested that the mitochondrial membrane proteins FUNDC1 and AMPK are closely related to mitochondrial function and mitophagy. In our study, we found that the expression level of FUNDC1 changed when IR injury disrupted mitochondrial function, and this effect was closely related to mitophagy. We also found that AMPK could regulate FUNDC1-related mitophagy, consistent with the findings of the study by Wu. However, unlike in Wu's study, the expression level of FUNDC1 decreased in our study, and AMPK regulated FUNDC1-dependent mitophagy through a change in phosphorylation. The differences between these studies may have been caused by the different model types and the existence of mitochondrial energy metabolism disorder, suggesting that different changes in FUNDC1 expression and regulatory pathways can occur under different conditions.

In summary, we found that tPA can repair mitochondrial function and decrease neuronal apoptosis via FUNDC1-mediated mitophagy, which may provide a new theoretical basis and therapeutic target for the clinical application of tPA. However, there were some limitations of this study. First, the downstream signaling pathways involved in FUNDC1-mediated mitochondrial autophagy were not investigated. Second, how tPA enters neurons and interacts with receptors was not explored in this study. The changes in neuronal mitophagy that occur after IR are part of a dynamic process dependent on the ischemia and reperfusion durations. This study failed to detect dynamic changes in mitophagy,

and it may thus have missed some effects of tPA in the IR process. As a result of these limitations, this study is unable to provide complete theoretical support for the clinical application of tPA. Such support should be pursued in future experiments.

Declaration of competing interest

The authors have reported that no competing interests exist in this work.

Acknowledgments

This work was supported by the National Natural Science Foundation of China (No. 81671169) and the Tianjin Science and Technology Commission (No. 17JCZDJC36500).

Appendix A. Supplementary data

Supplementary data to this article can be found online at https://doi.org/10.1016/j.redox.2020.101792.

References

[1] V. Jeanneret, M. Yepes, Tissue-type plasminogen activator is a homeostatic regulator of synaptic function in the central nervous system, Neural. Regen. Res. 12 (2017) 362–365, https://doi.org/10.4103/1673-5374.202924.
[2] M. Yepes, The plasminogen activation system promotes neurorepair in the ischemic brain, Curr. Drug Targets 20 (2019) 953–959, https://doi.org/10.2174/1389450120666181211144550.
[3] M. Louessard, A. Lacroix, M. Martineau, G. Mondielli, A. Montagne, F. Lesept, et al., Tissue plasminogen activator expression is restricted to subsets of excitatory pyramidal glutamatergic neurons, Mol. Neurobiol. 53 (2016) 5000–5012, https://doi.org/10.1007/s12035-015-9432-7.
[4] S.H. Lee, H.M. Ko, K.J. Kwon, Jongmin Lee, S.H. Han, D.W. Han, et al., tPA regulates neurite outgrowth by phosphorylation of LRP5/6 in neural progenitor cells, Mol. Neurobiol. 49 (2014) 199–215, https://doi.org/10.1007/s12035-013-8511-x.
[5] V. Jeanneret, F. Wu, P. Merino, E. Torre, A. Diaz, L. Cheng, et al., Tissue-type plasminogen activator (tPA) modulates the postsynaptic response of cerebral cortical neurons to the presynaptic release of glutamate, Front. Mol. Neurosci. 9 (2016) 121, https://doi.org/10.3389/fnmol.2016.00121.
[6] Yepes M, Tissue-type plasminogen activator is a neuroprotectant in the central nervous system, Front. Cell. Neurosci. 9 (2015) 304, https://doi.org/10.3389/fncel.2015.00304.
[7] L.L. Li, J. Tan, Y.Y. Miao, P. Lei, Q. Zhang, ROS and Autophagy: interactions and molecular regulatory mechanisms, Cell. Mol. Neurobiol. 35 (2015) 615–621, https://doi.org/10.1007/s10571-015-0166-x.
[8] B. Vurusaner, S. Gargiulo, G. Testa, G. Gamba, G. Leonarduzzib, G. Poli, et al., The role of autophagy in survival response induced by 27-hydroxycholesterol in human promonocytic cells, Redox Biol. 17 (2018) 400–410, https://doi.org/10.1016/j.redox.2018.05.010.
[9] W.H. Li, Y.J. Li, S. Siraj, H.J. Jin, Y.Y. Fan, X.R. Yang, et al., FUN14 domain-containing 1-mediated mitophagy suppresses hepatocarcinogenesis by inhibition of inflammasome activation in mice, Hepatology 69 (2019) 604–621, https://doi.org/10.1002/hep.30191.
[10] L. Liu, D. Feng, G. Chen, M. Chen, Q.X. Zheng, P.P. Song, et al., Mitochondrial outer-membrane protein FUNDC1 mediates ischemic-induced mitophagy in mammalian cells, Nat. Cell Biol. 14 (2012) 177–185, https://doi.org/10.1038/ncb2422.
[11] M. Matzingera, K. Fischhubera, D. Pölöskea, K. Mechtlerb, E.H. Heiss, AMPK leads to phosphorylation of the transcription factor Nrf2, tuning transactivation of selected target genes, Redox Biol. 29 (2020), https://doi.org/10.1016/j.redox.2019.101393, 101393.
[12] S. Jiang, T. Li, T. Ji, W. Yi, Z. Yang, S. Wang, et al., AMPK: potential therapeutic target for ischemic stroke, Theranostics 8 (2018) 4535–4551, https://doi.org/10.7150/thno.25674.
[13] F. Wu, A.D. Nicholson, W.B. Haile, E. Torre, J. An, C. Chen, et al., Tissue-type plasminogen activator mediates neuronal detection and adaptation to metabolic stress, J. Cerebr. Blood Flow Metabol. 33 (2013) 1761–1769, https://doi.org/10.1038/jcbfm.2013.124.
[14] J. An, W.B. Haile, F. Wu, E. Torre, M. Yepes, Tissue-type plasminogen activator mediates neuroglial coupling in the central nervous system, Neuroscience 257 (2014) 41–48, https://doi.org/10.1016/j.neuroscience.2013.10.060.
[15] W.B. Haile, J.L. Wu, R. Echeverry, F. Wu, J. An, M. Yepes, Tissue-type plasminogen activator has a neuroprotective effect in the ischemic brain mediated by neuronal TNF-α, J. Cerebr. Blood Flow Metabol. 32 (2012) 57–69, https://doi.org/10.1038/jcbfm.2011.106.
[16] A.M. Thiebaut, M. Gauberti, C. Ali, S. Martinez De Lizarrondo, D. Vivien, M. Yepes, et al., The role of plasminogen activators in stroke treatment: fibrinolysis and beyond, Lancet Neurol. 17 (2018) 1121–1132, https://doi.org/10.1016/S1474-4422(18)30323-5.
[17] E.Y. Yang, Y. Cai, X.H. Yao, J. Liu, Q.X. Wang, W.L. Jin, et al., Tissue plasminogen activator disrupts the blood-brain barrier through increasing the inflammatory response mediated by pericytes after cerebral ischemia, Aging (Albany NY) 11 (2019) 10167–10182, https://doi.org/10.18632/aging.102431.
[18] C.C. Wei, Y.Y. Kong, X. Hua, G.Q. Li, S.L. Zheng, M.H. Cheng, et al., NAD replenishment with nicotinamide mononucleotide protects blood-brain barrier integrity and attenuates delayed tissue plasminogen activator-induced haemorrhagic transformation after cerebral ischaemia, Br. J. Pharmacol. 174 (2017) 3823–3836, https://doi.org/10.1111/bph.13979.
[19] H.N. Kim, T.Y. Kim, Y.H. Yoon, J.Y. Koh, Pyruvate and cilostazol protect cultured rat cortical pericytes against tissue plasminogen activator (tPA)-induced cell death, Brain Res. 1628 (Pt B) (2015) 317–326, https://doi.org/10.1016/j.brainres.2015.06.022.
[20] R. Echeverry, J.L. Wu, W.B. Haile, J. Guzman, M. Yepes, Tissue-type plasminogen activator is a neuroprotectant in the mouse hippocampus, J. Clin. Invest. 120 (2010) 2194–2205, https://doi.org/10.1172/JCI41722.
[21] F. Wu, R. Echeverry, J.L. Wu, J. An, W.B. Haile, D.S. Cooper, et al., Tissue-type plasminogen activator protects neurons from excitotoxin-induced cell death via activation of the ERK1/2-CREB-ATF3 signaling pathway, Mol. Cell. Neurosci. 52 (2013) 9–19, https://doi.org/10.1016/j.mcn.2012.10.001.
[22] F. Wu, J. Wu, A.D. Nicholson, R. Echeverry, W.B. Haile, M. Catano, et al., Tissue-type plasminogen activator regulates the neuronal uptake of glucose in the ischemic brain, J. Neurosci. 32 (2012) 9848–9858, https://doi.org/10.1523/JNEUROSCI.1241-12.2012.
[23] J.H. Feng, X.M. Chen, J.G. Shen, Reactive nitrogen species as therapeutic targets for autophagy: implication for ischemic stroke, Expert Opin. Ther. Targets 21 (3) (2017 Mar) 305–317, https://doi.org/10.1080/14728222.2017.1281250.
[24] X.G. Zhang, H.J. Yan, Y. Yuan, J.Q. Gao, Z. Shen, Y. Cheng, et al., Cerebral ischemia-reperfusion induced autophagy protects against neuronal injury by mitochondrial clearance, Autophagy 9 (9) (2013 Sep) 1321–1333, https://doi.org/10.4161/auto.25132.
[25] Q. He, Z.Y. Li, C.C. Meng, J.X. Wu, Y. Zhao, J. Zhao, Parkin-dependent mitophagy is required for the inhibition of ATF4 on NLRP3 inflammasome activation in cerebral ischemia-reperfusion injury in rats, Cells 8 (8) (2019 Aug 14) E897, https://doi.org/10.3390/cells8080897.
[26] S.H. Baek, A.R. Noh, K.A. Kim, M. Akram, Y.J. Shin, E.S. Kim, et al., Modulation of mitochondrial function and autophagy mediates carnosine neuroprotection against ischemic brain damage, Stroke 45 (8) (2014 Aug) 2438–2443, https://doi.org/10.1161/STROKEAHA.114.005183.
[27] J.H. Feng, X.M. Chen, B.H. Guan, C.M. Li, J.H. Qiu, J.G. Shen, Inhibition of peroxynitrite-induced mitophagy activation attenuates cerebral ischemia-reperfusion injury, Mol. Neurobiol. 55 (8) (2018 Aug) 6369–6386.
[28] Q. Li, T. Zhang, J. Wang, Z.J. Zhang, Y. Zhai, G.Y. Yang, et al., Rapamycin attenuates mitochondrial dysfunction via activation of mitophagy in experimental ischemic stroke, Biochem. Biophys. Res. Commun. 444 (2) (2014 Feb 7) 182–188, https://doi.org/10.1016/j.bbrc.2014.01.032.
[29] M.E. Diaz-Casado, E. Lima, J.A. Garcia, C. Doerrier, P. Aranda, R.K. Sayed, et al., Melatonin rescus zebrafifish embryos from the parkinsonian phenotype restoring the parkin/PINK1/DJ-1/MUL1 network, J. Pineal Res. 61 (2016) 96–107, https://doi.org/10.1111/jpi.12332.
[30] H. Zhou, P.J. Zhu, J. Guo, N. Hu, S.Y. Wang, D.D. Li, et al., Ripk3 induces mitochondrial apoptosis via inhibition of FUNDC1 mitophagy in cardiac IR injury, Redox Biol. 13 (2017) 498–507, https://doi.org/10.1016/j.redox.2017.07.007.
[31] S. Wu, Q. Lu, Y. Ding, Y. Wu, Y. Qiu, P. Wang, et al., Hyperglycemia-driven inhibition of amp-activated protein kinase α2 induces diabetic cardiomyopathy by promoting mitochondria-associated endoplasmic reticulum membranes in vivo, Circulation 139 (2019) 1913–1936, https://doi.org/10.1161/CIRCULATIONAHA.118.033552.